Supporting Information File

Specific detection of proteins by a nanobody-functionalized nanopore sensor

Xialin Zhang[1], Nicole Stéphanie Galenkamp[2], Nieck Jordy van der Heide[2], Julián Valero Moreno[1,4], Giovanni Maglia[2,3,*], Jørgen Kjems[1,4,*]

[1]Interdisciplinary Nanoscience Center, Aarhus University, Aarhus C 8000, Denmark

[2]Groningen Biomolecular Science & Biotechnology Institute and [3]Center for Systems Chemistry, Stratingh Institute for Chemistry, University of Groningen, Nijenborg 4, 9747 AG, Groningen, Netherlands

[4]Department of Molecular Biology and Genetics, Aarhus University, Aarhus C 8000, Denmark.

*Correspondence author: Email: jk@mbg.au.dk; Email: giovanni.maglia@rug.nl

Competing interests: The authors have declared that no competing interests exist. G.M. is a founder, director, and shareholder of Portal Biotech Limited, a company engaged in the development of nanopore technologies. This work was not supported by Portal Biotech Limited.

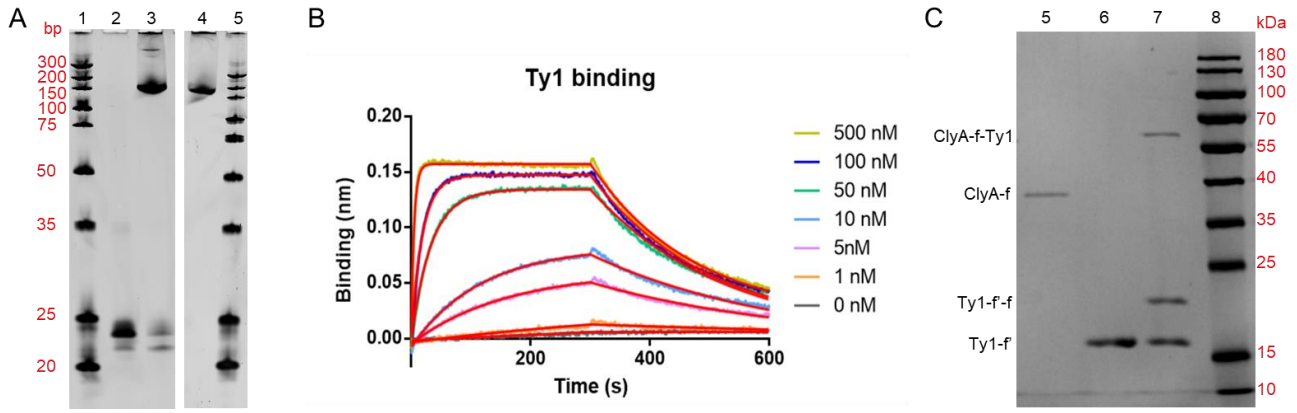

Figure S1. The conjugation of Ty1 nanobody with oligo f'. (A) Urea gel analysis of Ty1-f' conjugation. Lane 1 and 5: URL DNA ladder, lane 2: f'-DBCO, lane 3: mix of f'-DBCO with 5x azide-modified Ty1 nanobody after reacting overnight, lane 4: Ty1-f' conjugates purified by ion exchange chromatography. (B) BLI analysis of oligo-attached Ty1 binding to the Spike RBD domain. At the BLI experimental condition (150 mM NaCl, 50 mM Tris-HCl, pH 7.5), we measured the binding K_d to 9 nM, which is similar to the reported K_ds of 8 ± 1.5 and 13 ± 1.5 nM at 280 mM and 680 mM (high salt) conditions, respectively[1]. Although the salt conditions of the BLI experiments were slightly different, we conclude that the binding affinity of Ty1 is not significantly affected by the attached oligo. The binding curves were fitted using a nonlinear regression program (Association then dissociation) built in GraphPad Prism.

The kinetic data were obtained after the fitting. (C) SDS-PAGE analysis of the hybridization of ClyA-f with nanobody conjugates Ty1-f'. Lane 5, unpurified ClyA-f conjugates, lane 6: purified Ty1-f' conjugates, lane 7: annealing product of unpurified ClyA-f with 5-fold excess of purified Ty1-f'. The band of Ty1-f'-f was caused by free f oligo in unpurified ClyA-f sample hybridizing with Ty1-f'.

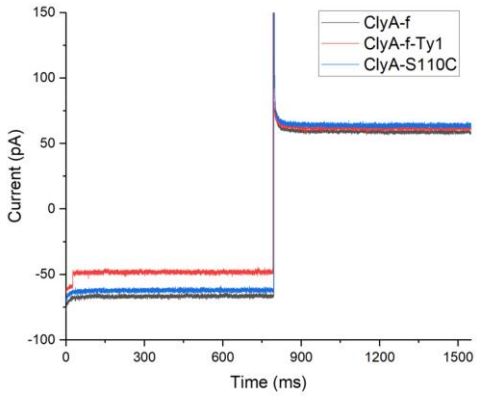

Figure S2. Representative current traces of ClyA-S110C, ClyA-f, ClyA-f-Ty1 at applied potentials of -35 and 35 mV. These experiments were performed in 150 mM NaCl, 50 mM Tris-HCl, pH 7.5.

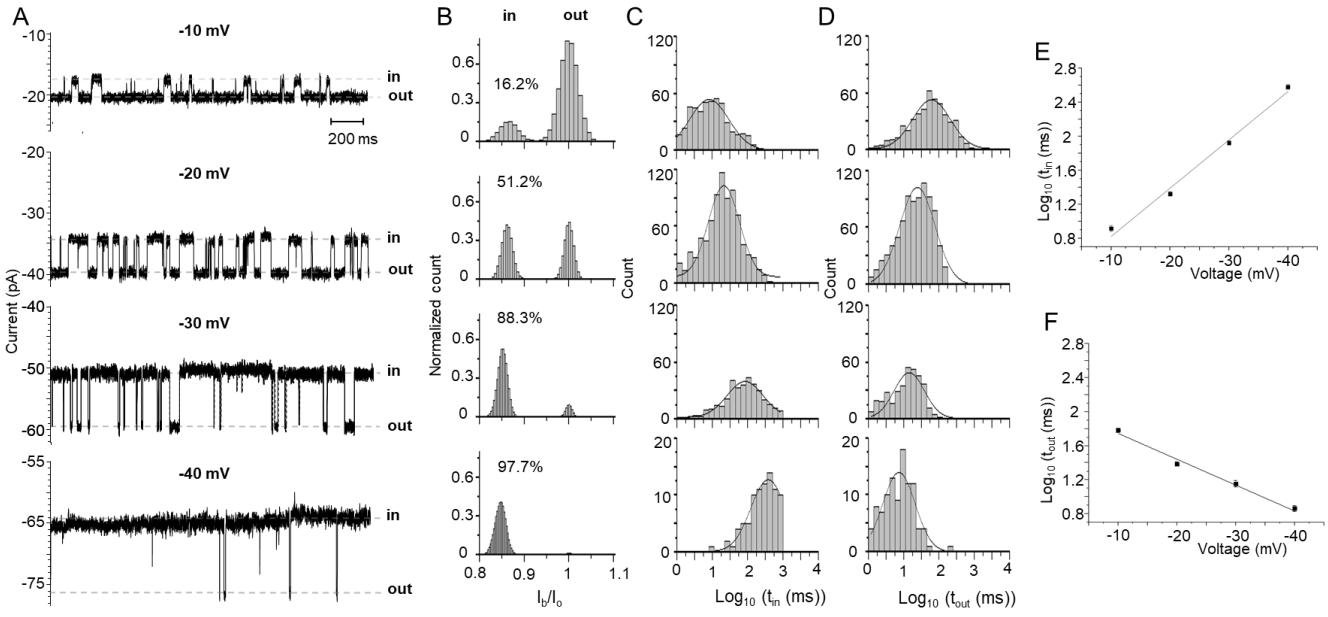

Figure S3. Single channel recording traces of ClyA-f-Ty1 and the analysis of residual current I_b/I_o, t_{in} and t_{out} under different applied potentials. (A) Representative current traces of ClyA-f-Ty1 under applied potentials ranging from

-10 to -40 mV. (B) All-point histogram of current traces in A, showing Ty1 nanobodies tend to reside in ClyA nanopore with increasing applied potentials. (C, D) Histogram of logarithmic time of Ty1 locating inside and outside of ClyA, respectively. The histograms were fitted with Gaussian distribution function. (E, F) The influence of applied potentials on the average logarithmic time of Ty1 locating inside and outside of ClyA. These experiments were performed in 150 mM NaCl, 50 mM Tris-HCl, pH 7.5.

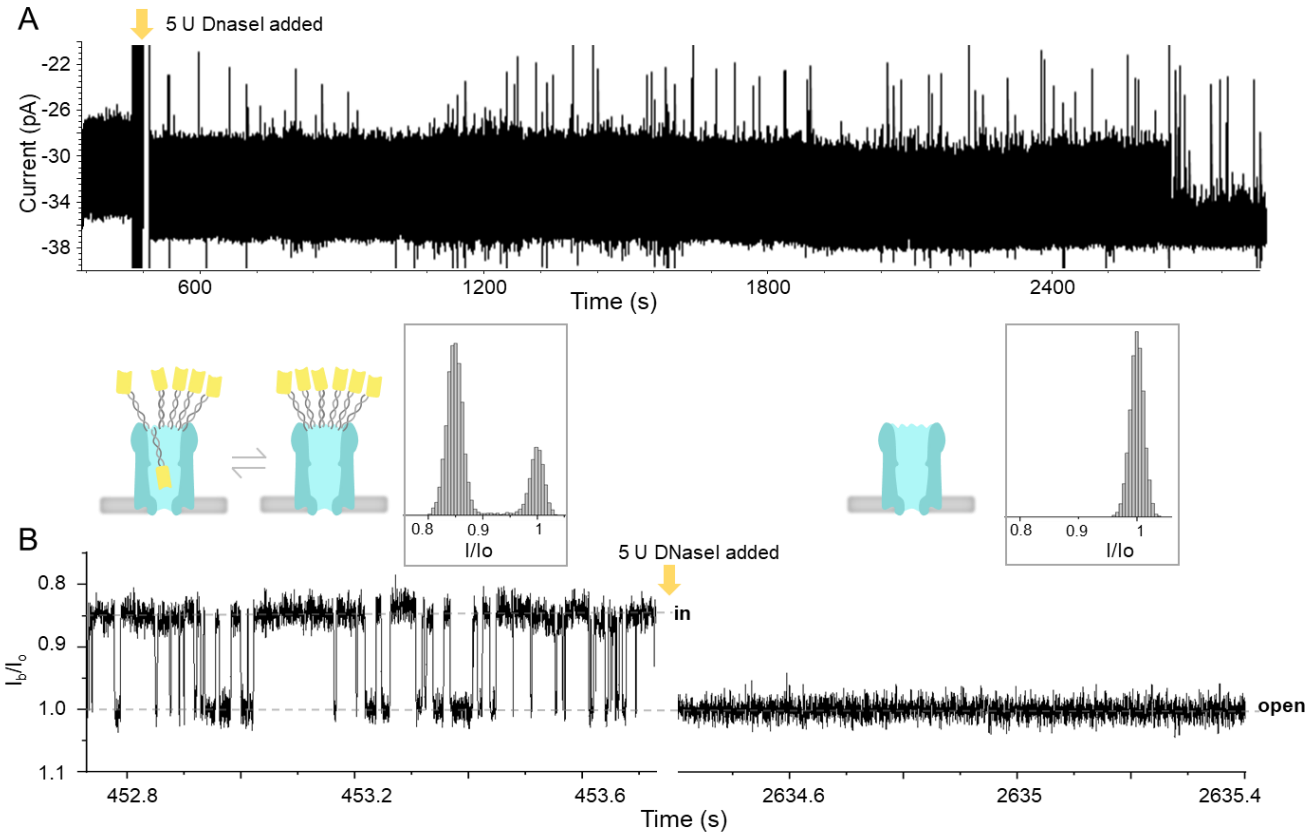

Figure S4. Verify the attachment of Ty1 on ClyA through DNA oligo hybridization using DNase I. (A) Current traces of ClyA-f-Ty1 before and after the addition of 5 U DNase I in the presence of 2.5 mM $MgCl_2$ at an applied potential of -20 mV. (B) Enlarged representative current traces from A, showing that the nanobodies attached to the ClyA nanopore were removed after the addition of DNase I for about 30 mins. All-point histograms were displayed on the top of the panel showing the current distribution before and after the addition of DNase I. Schematic model shown above depicts how the nanobodies were removed from ClyA nanopore. The experiments were performed in 150 mM NaCl, 2.5 mM $MgCl_2$, 50 mM Tris-HCl, pH 7.5.

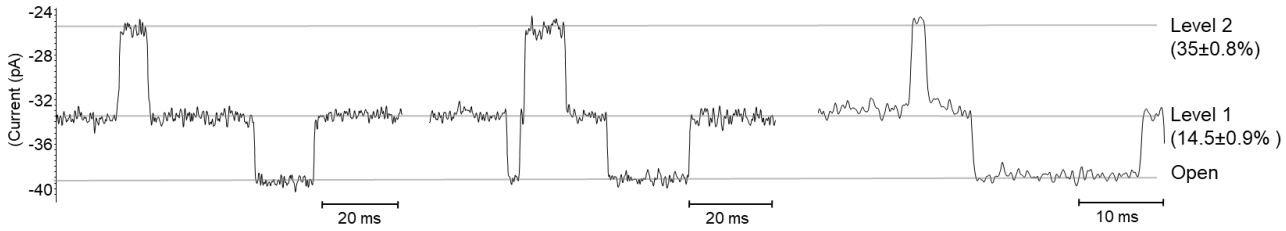

Figure S5. Two-level blockage signals observed in ClyA-f-Ty1 nanopore at an applied potential of -20 mV. These signals were caused by two Ty1 nanobodies residing in the ClyA nanopore. The experiments were performed in 150 mM NaCl, 50 mM Tris-HCl, pH 7.5.

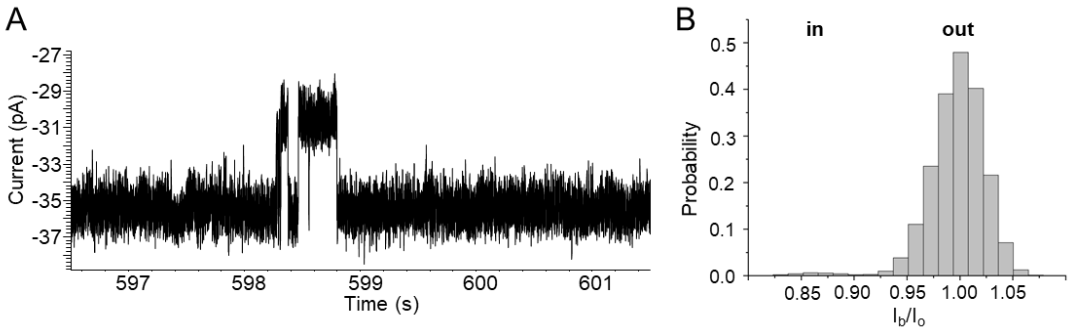

Figure S6. The conductive behavior of ClyA with less amount of Ty1. (A) Representative current blockades observed on ClyA when incubated with 100-fold diluted Ty1-f'. The current was recorded under an applied potential of -20 mV. The current blockade percentage was similar to that of fully equipped ClyA-f-Ty1, while the frequency of the blockade events was much lower. (B) All-point histogram of the current traces of ClyA attached with less amount of Ty1 nanobodies. The blocking probability was smaller than that of the fully equipped ClyA-f-Ty1.

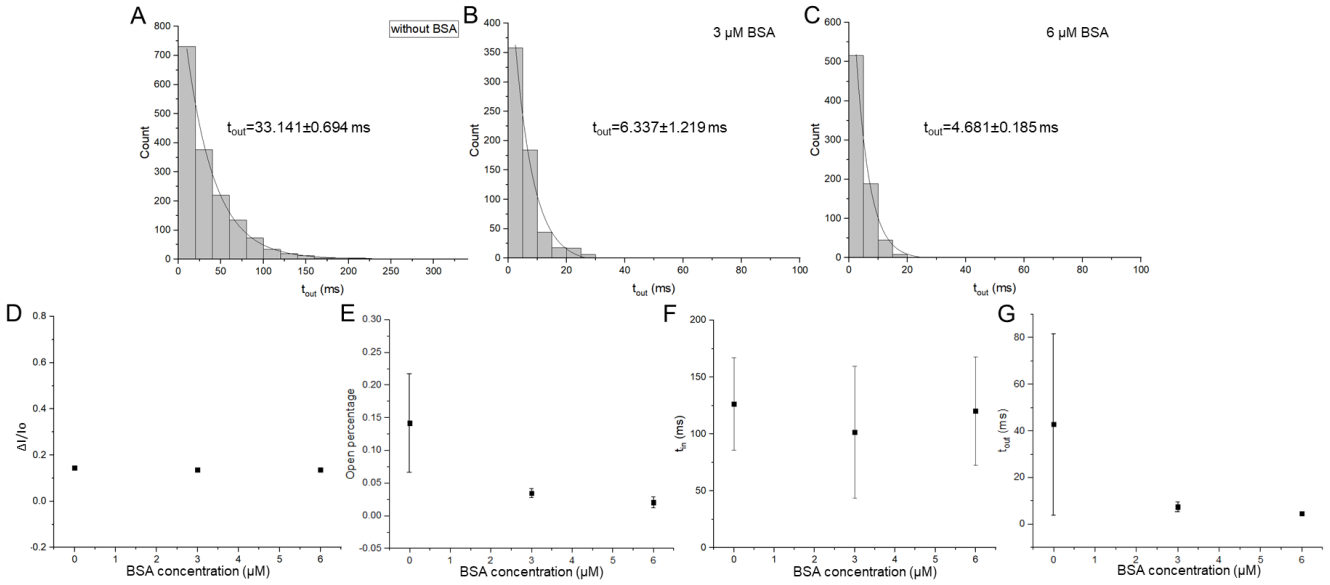

Figure S7. Effect of BSA on nanobody internalization. (A-C) Histograms distribution of t_{out} before and after the addition of 3 μM BSA, 6 μM BSA in *cis* location. The histograms were fitted with single exponential function. (D-G) The change of blockade percentage, open percentage, average time of Ty1 staying inside the ClyA nanopore (t_{in}), average time of Ty1 staying outside the ClyA nanopore (t_{out}) with increasing concentration of BSA, respectively. (n=4, each experiment was conducted with independent nanopores. Error bars represent standard deviations. Large standard error bars may reflect that the nanopores are equipped with slightly different number of nanobodies. These experiments were performed in 150 mM NaCl, 50 mM Tris-HCl, pH 7.5.

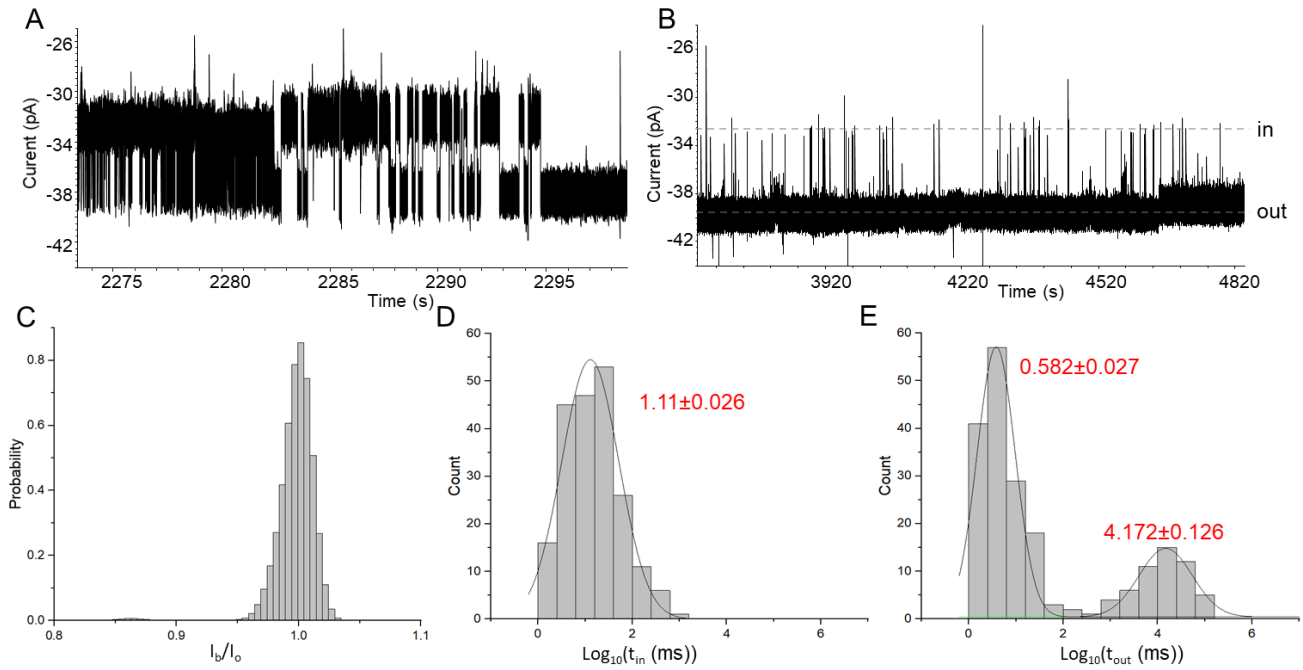

Figure S8. The effect of adding 2.3 nM Spike protein to the ClyA-f-Ty1 pore. (A) Current traces showed the transition of the pore from reversible blockade state to open state after the addition of 2.3 nM Spike protein. (B) In the presence of 2.3 nM Spike protein, the current traces of ClyA-f-Ty1 (recording time: 20 mins). The current shifts may reflect a sub-state of the ClyA nanopore as a result of the interaction of Spike protein and the nanopore. (C) All-point histogram of the current traces presented in B. (D, E) Histogram of the logarithm of t_{in} and t_{out} after the addition of 2.3 nM Spike protein in a recording time of 20 minutes. The histograms were fitted with Gaussian distribution functions. These experiments were performed in 150 mM NaCl, 50 mM Tris-HCl, pH 7.5 in the presence of 6 µM BSA in *cis*.

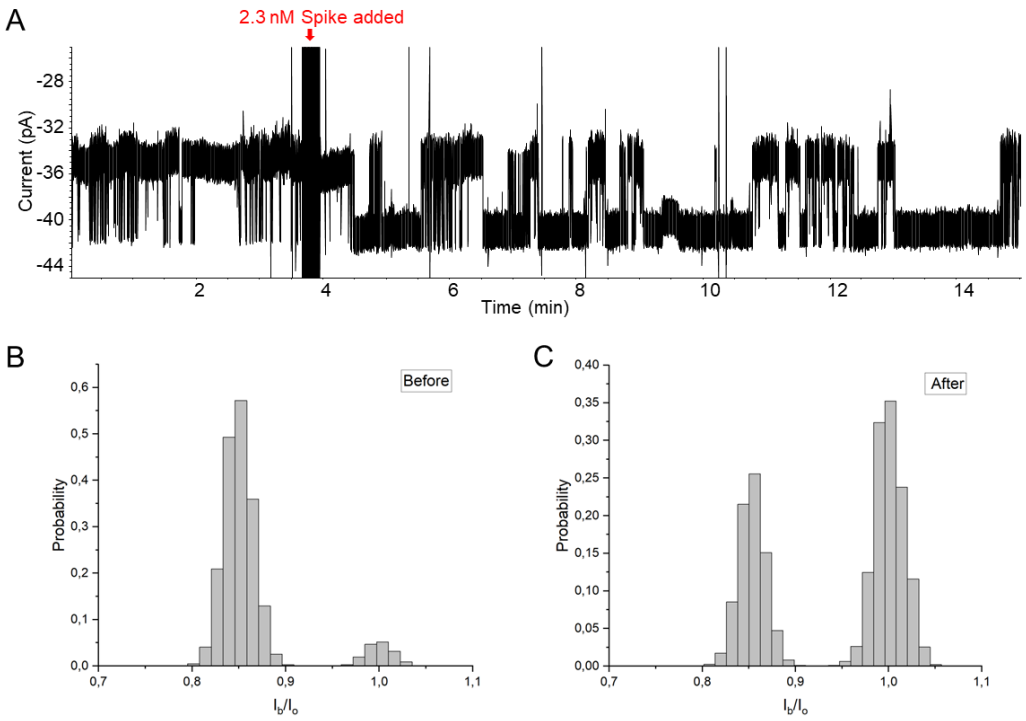

Figure S9. Spike protein detection in the absence of BSA. (A) The representative current traces of ClyA-f-Ty1 after the addition of 2.3 nM spike protein in the absence of BSA at an applied potential of -20 mV. (B, C) The all-point histogram of the current traces before (B) and after (C) adding 2.3 nM Spike in the absence of BSA. The addition of Spike led to the opening of ClyA-f-Ty1 nanopore with a probability increasing from 8% to 61%. The experiment was performed in 150 mM NaCl, 50 mM Tris-HCl, pH 7.5 in the absence of BSA.

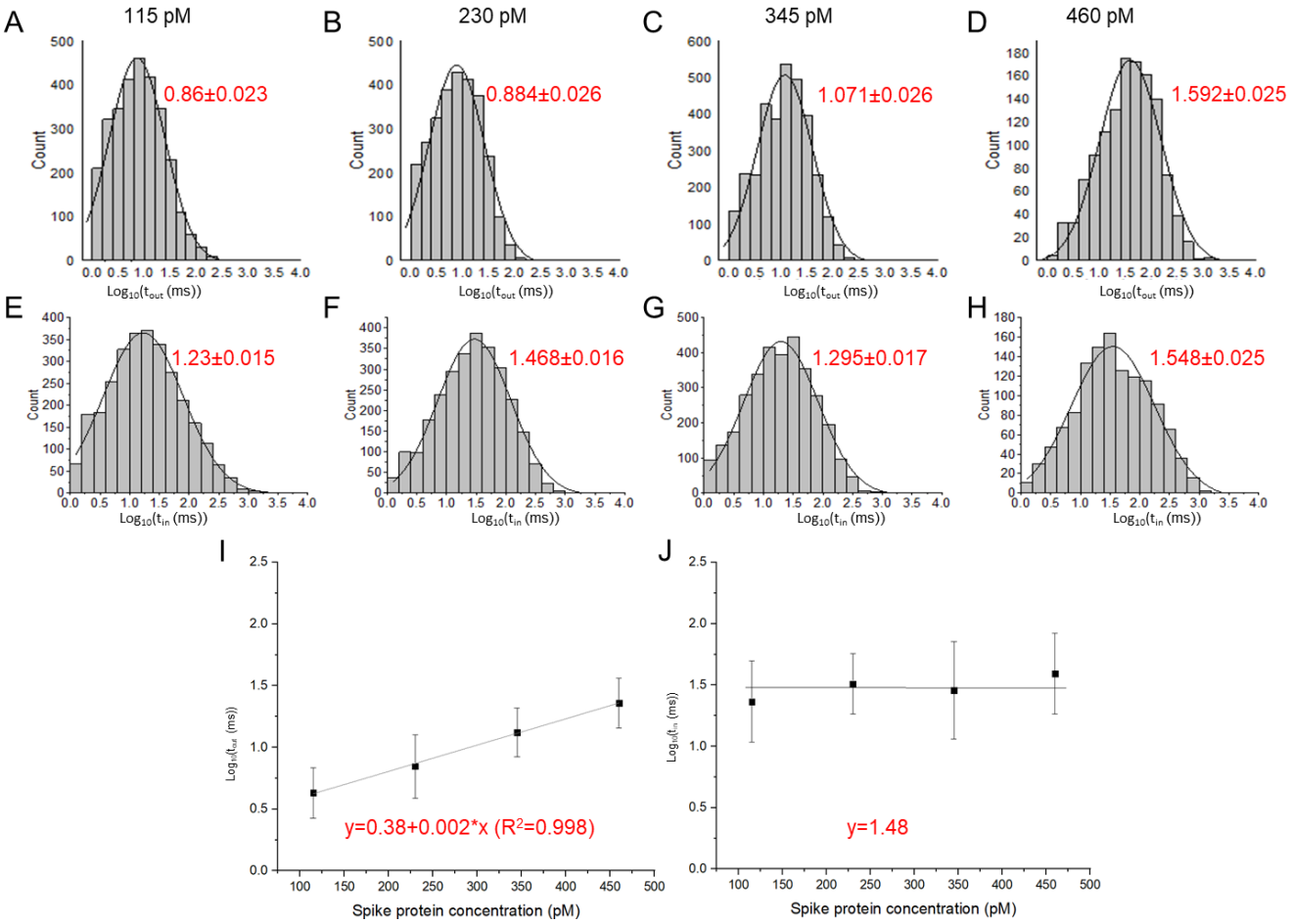

Figure S10. The influence of Spike proteins concentration on binding kinetics to the ClyA-f-Ty1 pore. (A-D) Histogram of $\log_{10}(t_{out})$ at Spike concentration of 115 pM, 230 pM, 345 pM, 460 pM, respectively. The data were fitted with Gaussian distribution. (E-H) Histograms of $\log_{10}(t_{in})$ at Spike concentration of 115 pM, 230 pM, 345 pM, 460 pM, respectively. The data were fitted with Gaussian distribution. (I, J) Concentration dependency of the logarithm of t_{out} and t_{in}. Large standard error bars may reflect that nanopores are equipped with a slightly different number of nanobodies. Despite the slight variance, t_{out} and t_{in} clearly respond to the Spike concentrations. These experiments were performed in 150 mM NaCl, 50 mM Tris-HCl, pH 7.5 in the presence of 6 µM BSA in *cis*.

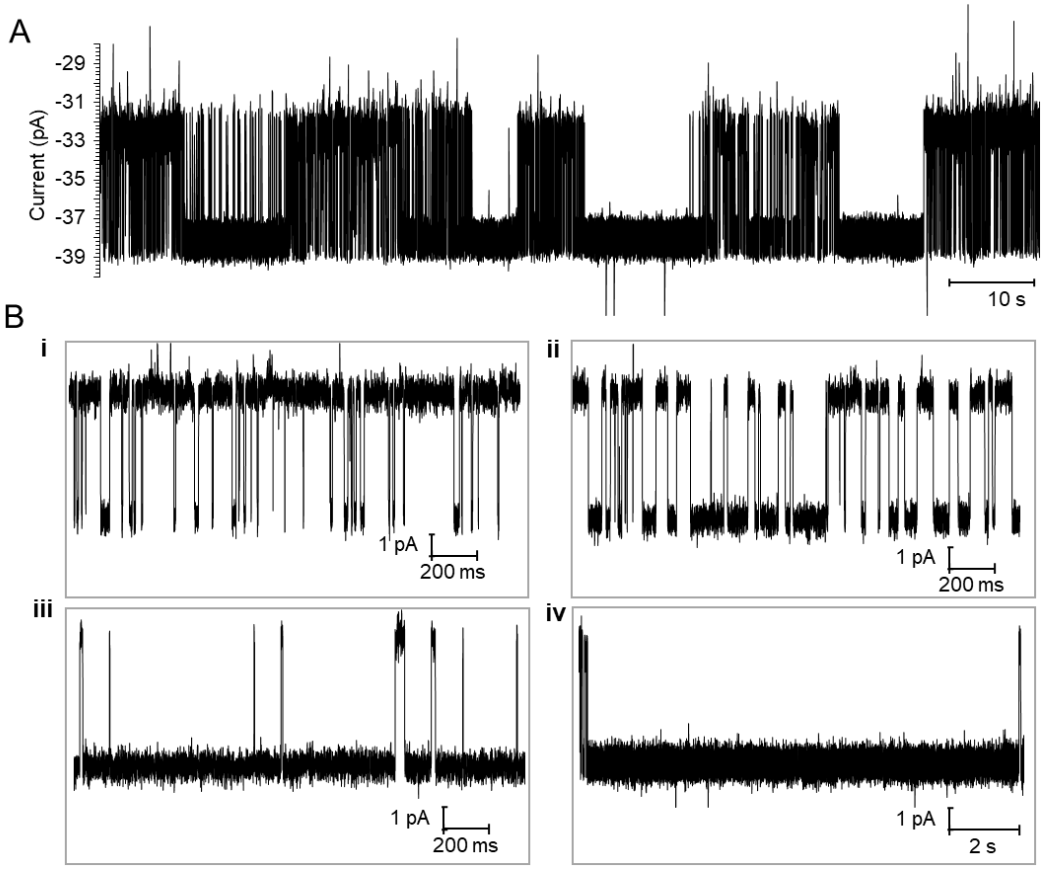

Figure S11. The conductive behavior of ClyA-f-Ty1 after adding 690 pM of Spike. (A) Current traces after adding 690 pM Spike in the presence of 6 µM BSA at -20 mV. (B) Different current trace patterns with various open times ranging from few milliseconds to tens of seconds after adding 690 pM Spike.

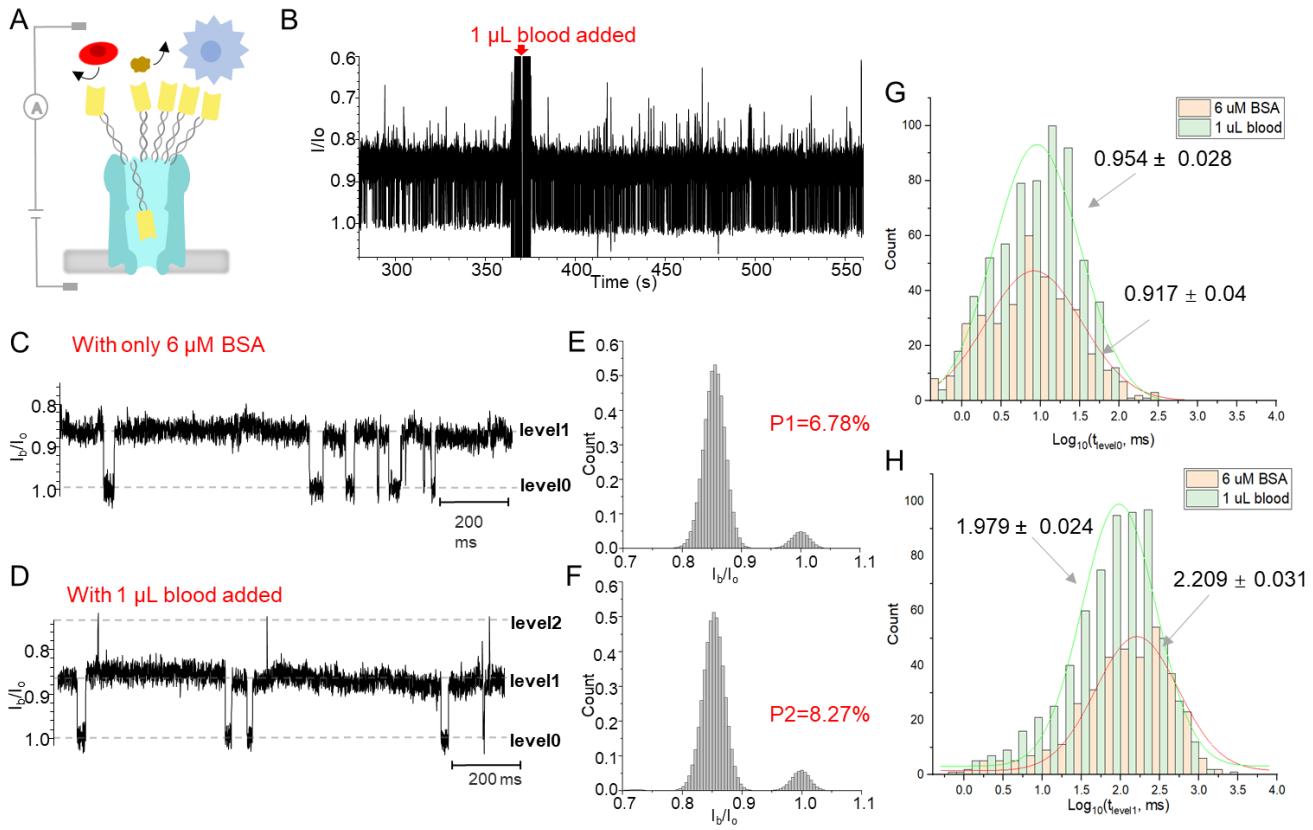

Figure S12. The behavior of ClyA-f-Ty1 in the presence of blood. (A) Schematic model showing electrical measurement of ClyA-f-Ty1 in the presence of blood. (B) Current traces showing the current change before and after addition of 1 µL of blood to the ClyA-f-Ty1 nanopore in 500 µL electrolyte buffer. (C, D) Representative current traces in the presence of 6 µM BSA (C) and after addition of 1 µL of blood (D). (E, F) All-point histograms of the current traces before (E) and after (F) addition of 1 µL of blood. (G) Histogram of the logarithm of dwell time in level0 before and after the addition of 1 µL of blood. (H) Histogram of the logarithm of dwell time in level1 before and after the addition of 1 µL of blood. These experiments were performed in electrolyte buffer 150 mM NaCl, 50 mM Tris-HCl, pH 7.5 in the presence of 6 µM BSA in *cis*.

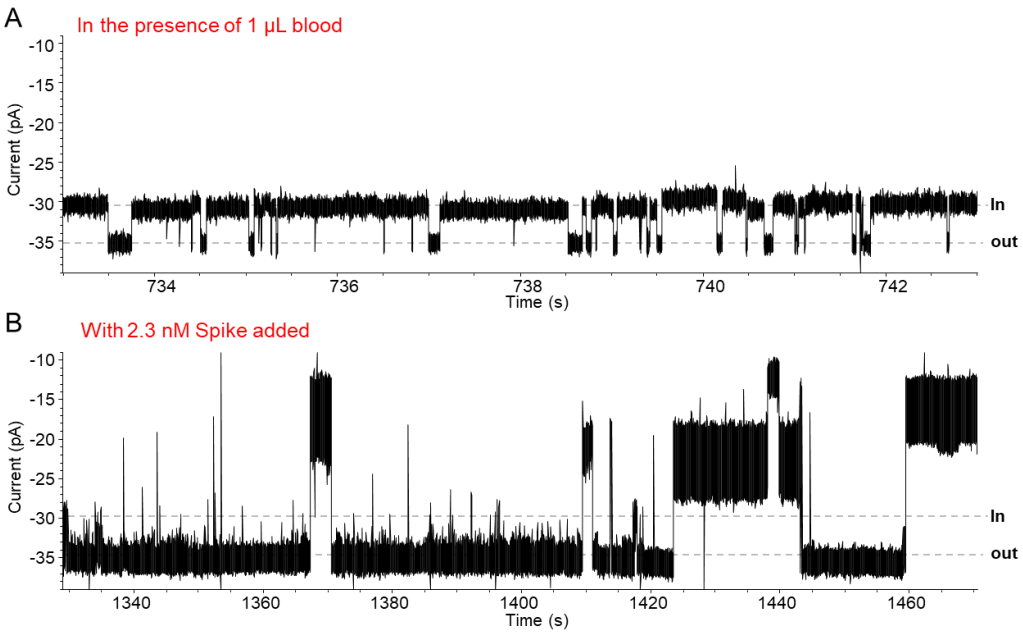

Figure S13. Detection of spike trimer using ClyA-f-Ty1 in the presence of blood. (A, B) Representative current traces before (A) and after (B) the addition of 2.3 nM Spike protein in the presence of 1 µL blood at a bias of -20 mV. The experiment was performed in 150 mM NaCl, 50 mM Tris-HCl, pH 7.5 in the presence of 6 µM BSA in *cis*.

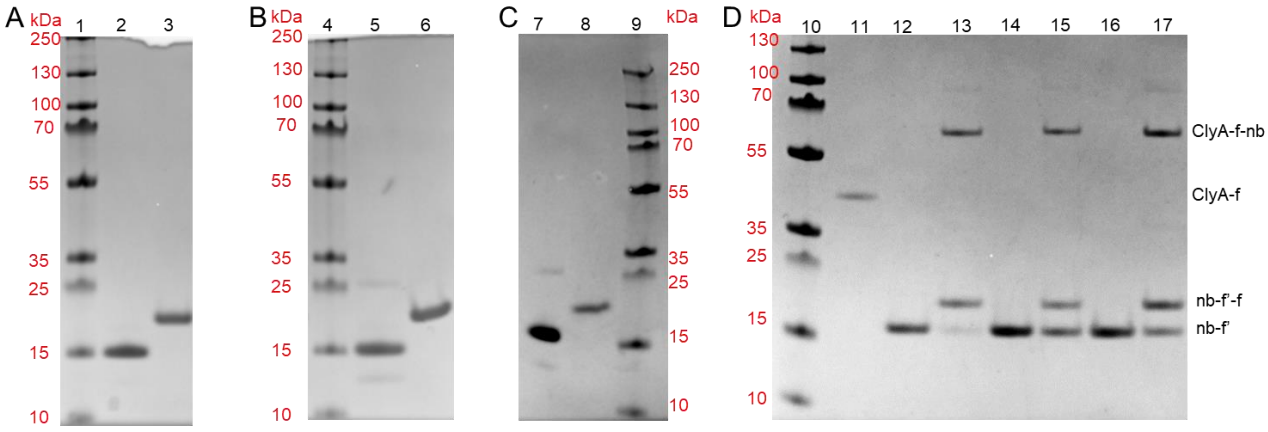

Figure S14. (A-C) SDS-PAGE gel analysis of the conjugation of nb22-f', 2Rb17c-f' and 2Rs15d-f' purified by ion exchange chromatography. Lane 1, 4, 9: protein ladder, lane 2: azide-modified nb22, lane 3: purified nb22-f' conjugates, lane 5: azide-modified 2Rb17c, lane 6: purified 2Rb17c-f' conjugates, lane 7: azide-modified 2Rs15d, lane 8: purified 2Rs15d-f' conjugates. (D) SDS-PAGE analysis of the hybridization of ClyA-f with nanobody conjugates 2Rs15d-f', 2Rb17c-f' and nb22-f'. Lane 10: protein ladder, lane 11: unpurified ClyA-f conjugates, lane 12, 14, 16: purified 2Rs15d-f', 2Rb17c-f' and nb22-f' conjugates, lane 13, 15, 17: annealing product of unpurified

ClyA-f with 5-fold excess of purified 2Rs15d-f', 2Rb17c-f' and nb22-f' conjugates, respectively. The band of ClyA-f was upshifted due to the attachment of nanobodies (nb).

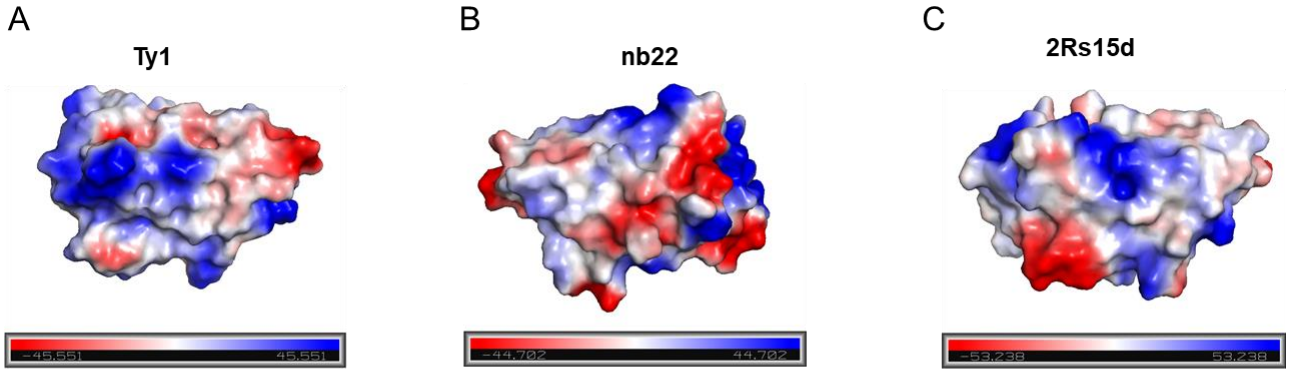

MW: 12.6 kDa
pI: 9.34
K_D (BLI, RBD): 5-9 nM
K_d (1/s): 4-5E-3

MW: 13.1 kDa
pI: 8.66
K_D (SPR): 0.2 nM
K_a (1/Ms): (4.6 ± 0.8)E+5
K_d (1/s):(7.8 ± 2.2) E-5

MW: 12.6 kDa
pI: 7.83
K_D (SPR): 2.7 nM
K_a (1/Ms): 2.14E+5
K_d (1/s): 5.71E-4

Figure S15. Surface charge distribution of nanobodies Ty1 (A, PDB: 6ZXN), nb22 (B, PDB: 5LHR), and 2Rs15d (C, PDB: 5MY6) and their information of molecular weight, pI and binding affinity. The crystal structure of 2Rb17c is not available.

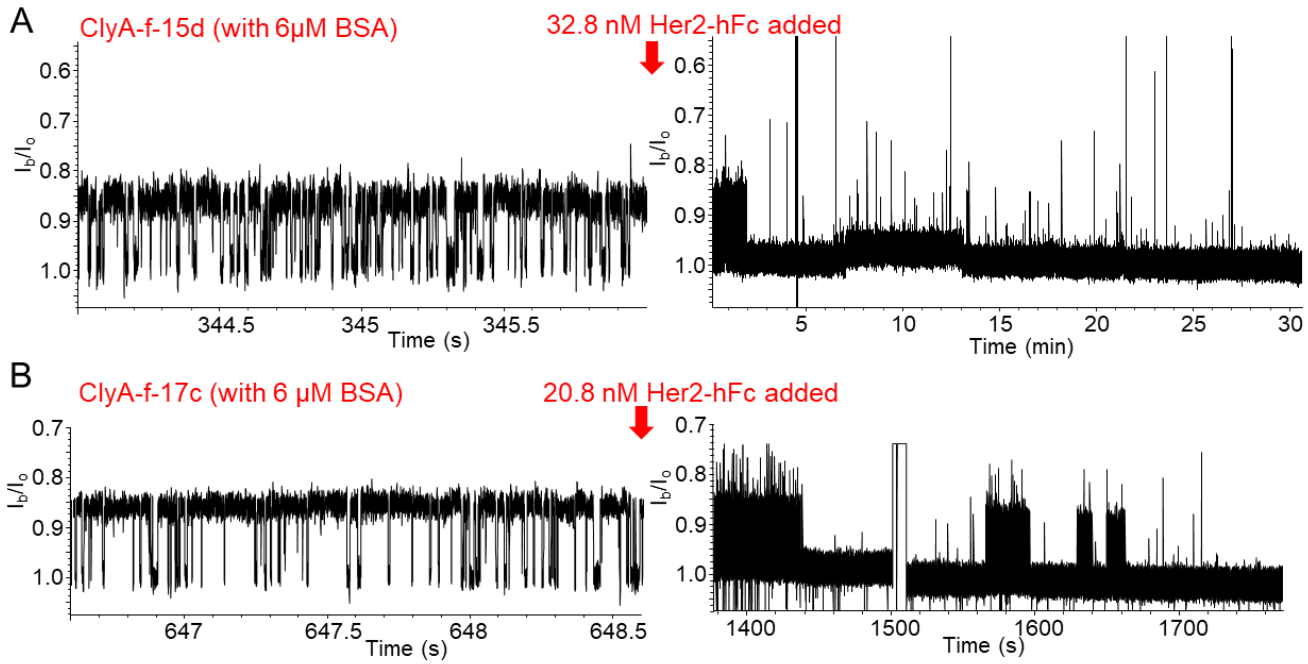

Figure S16. Detection of Her2 with ClyA-f-15d and ClyA-f-17c nanopores. (A) Representative current traces of ClyA attached by 2Rs15d nanobody (ClyA-f-15d) before and after the addition of 32.8 nM Her2 protein under an applied potential of -20 mV. Those current shifts might be a sub-state of the ClyA nanopore as a result of the interaction of protein and the nanopore. (B) Representative current traces of ClyA attached by 2Rb17c nanobody (ClyA-f-17c) before and after the addition of 20.8 nM Her2 protein at the same applied potential. Reported binding affinity of 2Rs15d to Her2: k_{on} = 2.14 x 10^5 M^{-1} s^{-1}, k_{off} = 5.71 x 10^{-4} s^{-1}, K_D = 2.7 nM. Reported binding affinity of 2Rb17c to Her2: k_{on} = 7.6 x 10^6 M^{-1} s^{-1}, k_{off} = 4.58 x 10^{-2} s^{-1}, K_D = 6 nM.[2] These experiments were performed in 150 mM NaCl, 50 mM Tris-HCl, pH 7.5 in the presence of 6 µM BSA in *cis*.

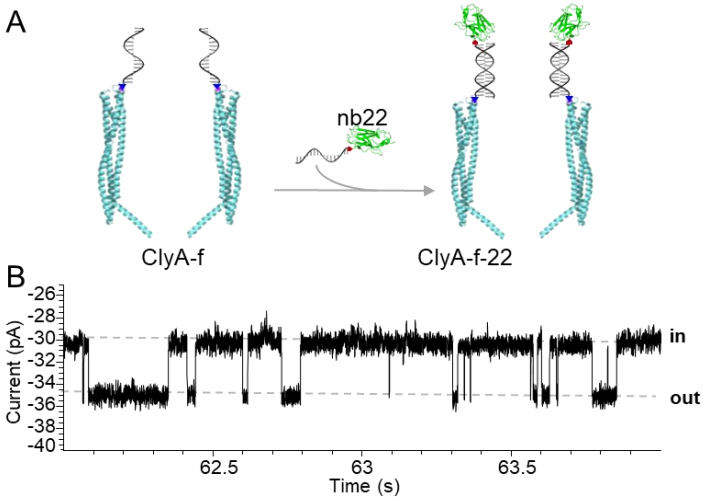

Figure S17. Electrical characterization of ClyA-f-nb22 nanopore. (A) Schematic model showing the strategy of functionalizing ClyA nanopore with nb22 nanobody. The nb22-f' conjugate was attached by annealing it to ClyA-f nanopore. (B) Representative current trace of ClyA-f-nb22 under an applied potential of -20 mV. "in" and "out" represents that one of the nb22 nanobodies attached on ClyA nanopore moves in and out of the pore's vestibule. The experiment was performed in 150 mM NaCl, 50 mM Tris-HCl, pH 7.5 in the presence of 6 µM BSA in *cis*.

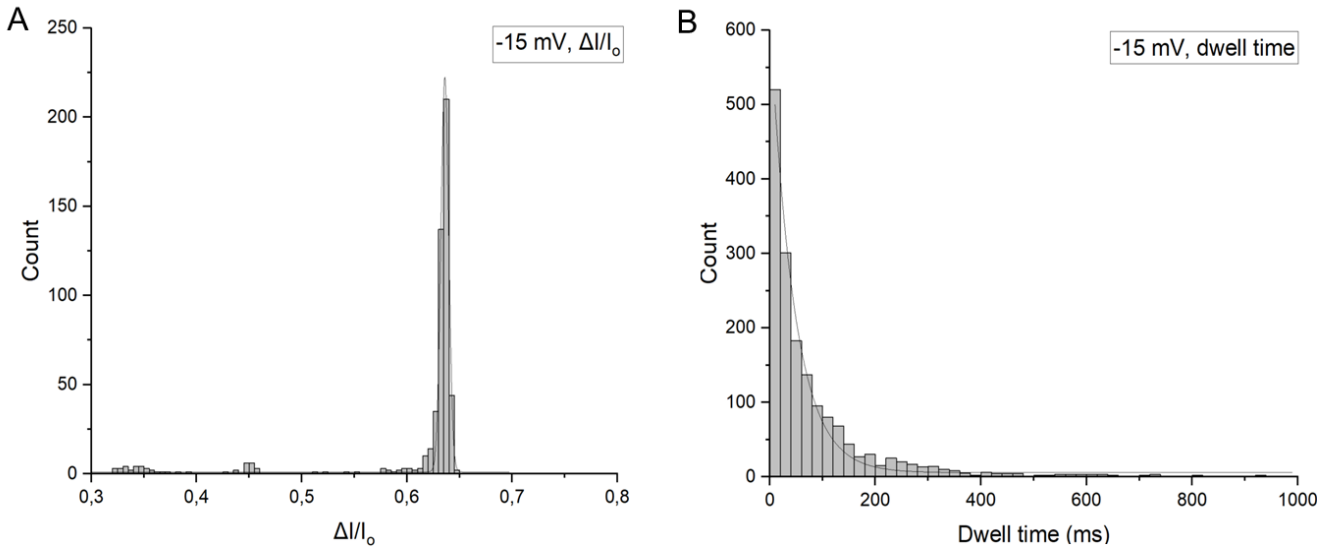

Figure S18. Statistics of the new class of blockade events caused by the addition of 3 nM muPA to ClyA-f-nb22 nanopore under -15 mV applied potential. (A) Histogram distribution of the current blockade (ΔI/Io) of the events. The plot was fitted by Gaussian function. (B) Histogram distribution of the dwell time of the events. The plot was fitted with exponential decay function.

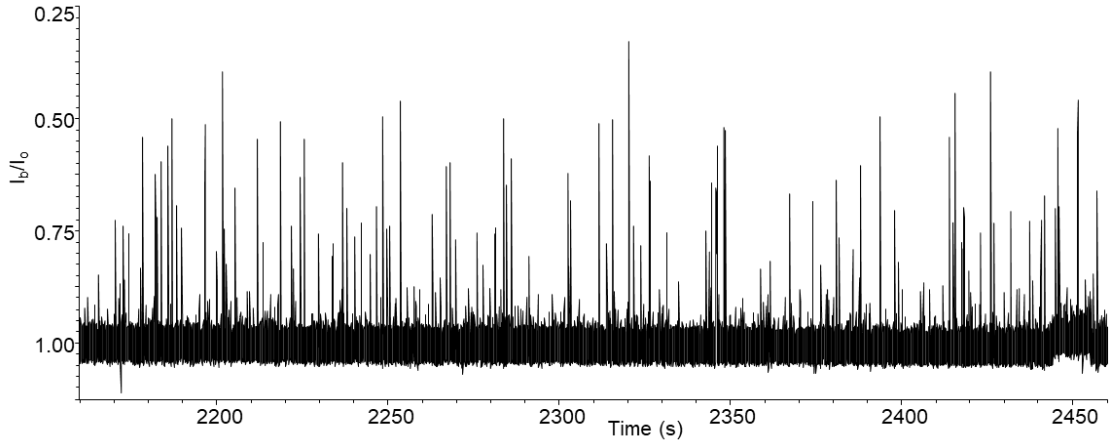

Figure S19. Representative current trace after the addition of 3 nM muPA to non-nanobody functionalized ClyA-f nanopore at an applied potential of -20 mV. The experiment was performed in 150 mM NaCl, 50 mM Tris-HCl, pH 7.5.

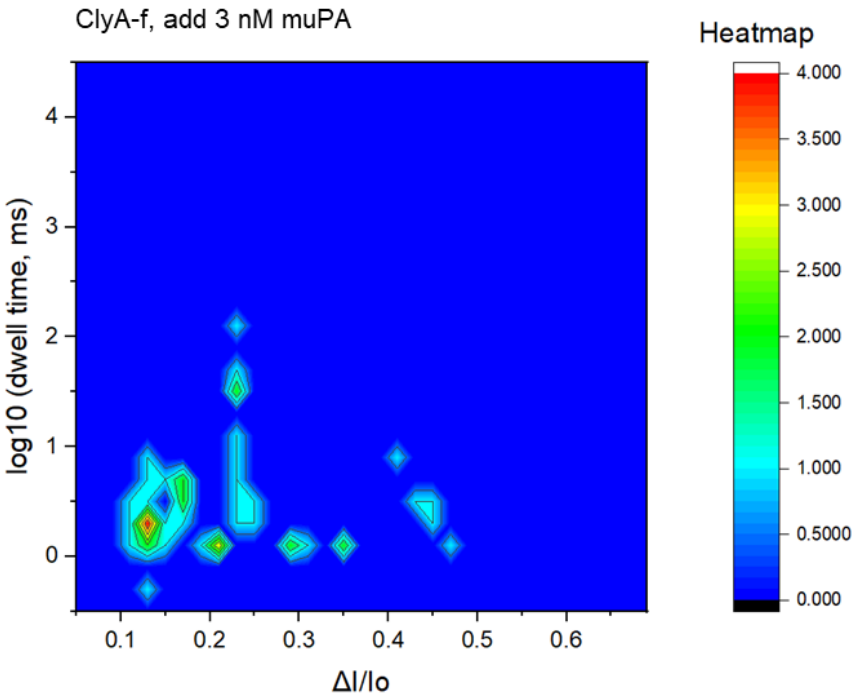

Figure S20. Heatmap of the blockade events observed after the addition of 3 nM muPA to non-nanobody functionalized ClyA-f nanopore with the logarithmic dwell time against current blockade (ΔI/Io).

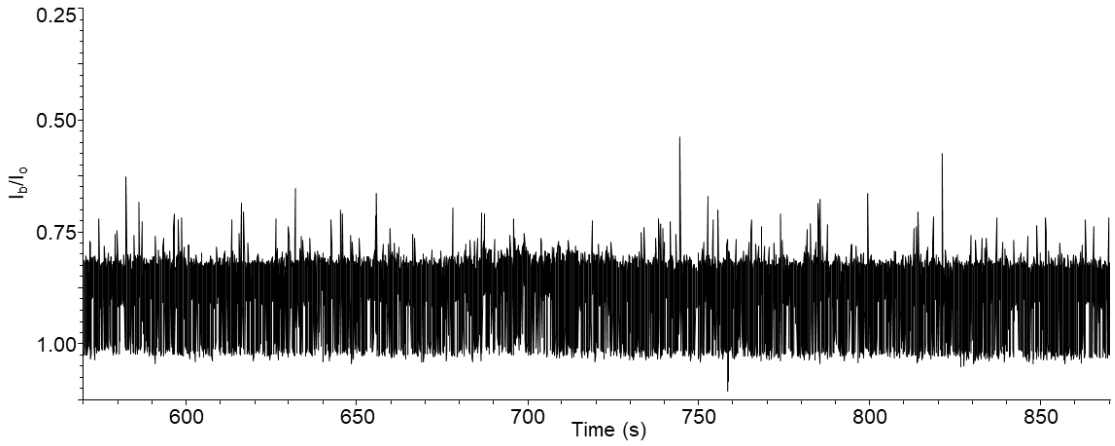

Figure S21. Representative current trace after the addition of 15 nM muPA to Ty1-nanobody functionalized ClyA-f-Ty1 nanopore at an applied potential of -20 mV. The experiment was performed in 150 mM NaCl, 50 mM Tris-HCl, pH 7.5.

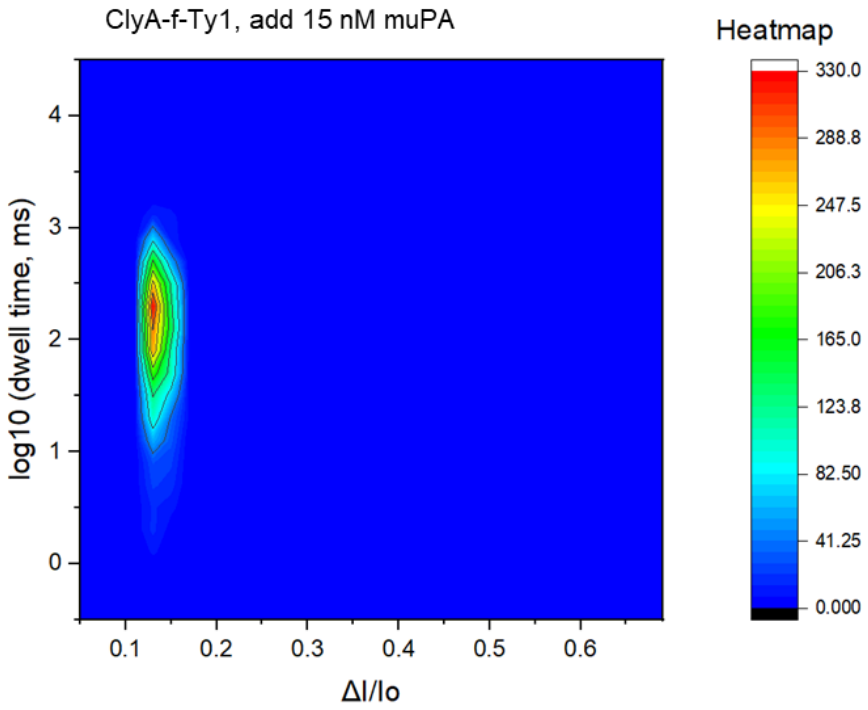

Figure S22. Heatmap of the blockade events observed after the addition of 15 nM muPA to ClyA-f-Ty1 nanopore with the logarithm of dwell time against current blockade (ΔI/Io).

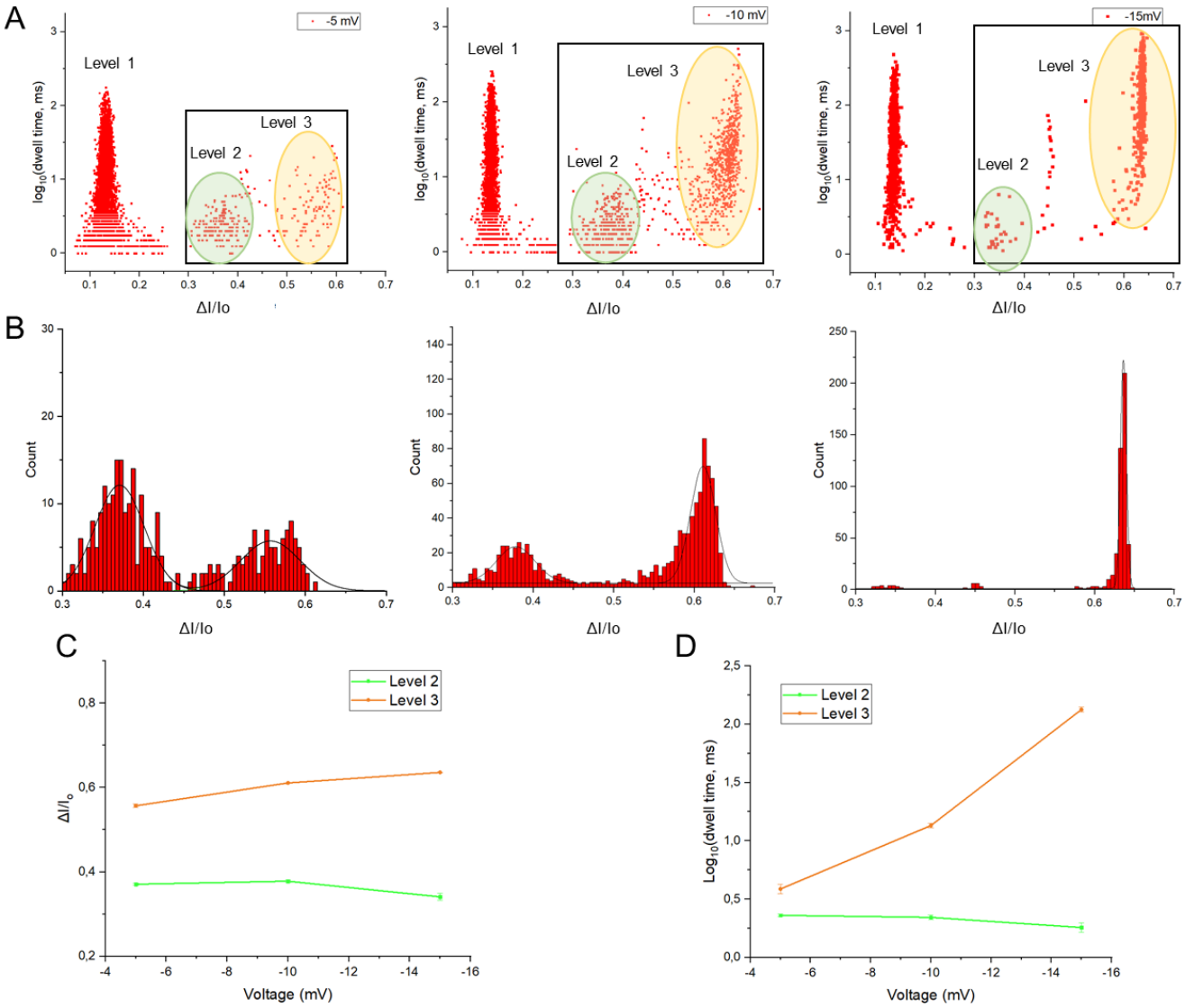

Figure S23. Amplitude, dwell time analysis of blockage signal induced by 3 nM muPA interacting with nb22 attached on ClyA nanopore under increasing applied potentials. (A) Scatter plots of the logarithm of dwell time versus current blockade (ΔI/Io) at -5, -10, -15 mV, respectively. (B) Histogram of current blockade distribution of the level 2 and level 3 events at -5, -10, -15 mV, respectively. (C, D) The influence of applied potentials on current blockade and the dwell time of the level 2 and level 3 events, respectively. The experiment was performed in 150 mM NaCl, 50 mM Tris-HCl, pH 7.5 in the presence of 6 µM BSA in *cis*.

Reference

1. Hanke, L. *et al.* An alpaca nanobody neutralizes SARS-CoV-2 by blocking receptor interaction. *Nat. Commun.* **11**, 4420 (2020).

2. Vaneycken, I. *et al.* Preclinical screening of anti-HER2 nanobodies for molecular imaging of breast cancer. *FASEB J.* **25**, 2433–2446 (2011).